Nano Energy 49 (2018) 316–323

Contents lists available at ScienceDirect

Nano Energy

journal homepage: www.elsevier.com/locate/nanoen

Communication

Enhancing the rate of electrochemical nitrogen reduction reaction for ammonia synthesis under ambient conditions using hollow gold nanocages

Mohammadreza Nazemi[a,b], Sajanlal R. Panikkanvalappil[a], Mostafa A. El-Sayed[a,*]

[a] Laser Dynamics Laboratory, School of Chemistry and Biochemistry, Georgia Institute of Technology, Atlanta, GA 30332-0400, United States
[b] George W. Woodruff School of Mechanical Engineering, Georgia Institute of Technology, Atlanta, GA, 30332-0405, United States

ARTICLE INFO

Keywords:
Nanocatalysis
Hollow gold nanocage
Nitrogen reduction reaction
Ammonia electrosynthesis
Cage effect

ABSTRACT

Ammonia production is imperative to increase the food supply for the growing global population. Ammonia is also considered a major hydrogen energy carrier. The current industrial method for ammonia production is energy intensive and heavily relies on fossil fuels, which are responsible for environmental pollution. To meet ammonia demands, it is necessary to develop sustainable and environmentally friendly production methods that consume significantly less energy than the current methods. The use of nanocatalysis in an electrochemical system under ambient conditions can make an alternative route for fertilizer production. Here, the use of hollow gold nanocages (AuHNCs) as an effective electrocatalyst is evaluated for electrochemical nitrogen reduction reaction (NRR) under ambient conditions. The electrochemical experiments are carried out at various potentials in 0.5 M $LiClO_4$ aqueous solution using AuHNCs, and their catalytic efficiency is determined for the conversion of nitrogen to ammonia. The highest ammonia Faradaic efficiency (30.2%) is achieved at − 0.4 V vs. RHE while the highest ammonia yield (3.9 μg cm^{-2} h^{-1}) is obtained at − 0.5 V vs. RHE. These are greater than the highest values currently reported in the literature in aqueous solution under ambient conditions. Furthermore, the role of temperature on the electrochemical NRR performance is evaluated. It is found that by increasing the operating temperature from 20 °C to 50 °C at − 0.4 V vs. RHE, the ammonia Faradaic efficiency increases from 30.2% at 20 °C to 40.5% at 50 °C. The electrocatalytic activity of NRR using AuHNCs is further compared with that of solid Au nanoparticles of various shapes (i.e., rods, spheres or cubes) to elucidate the enhanced rate of the reaction resulting from the increase in surface area and confinement effects. The three-fold enhancement in ammonia Faradaic efficiency is achieved by using the AuHNCs (30.2%) compared to the solid Au nanocubes (11.4%).

1. Introduction

Ammonia is the second most produced chemical in the world. The global production of ammonia approached ~146 million metric tons in 2015 and is projected to rise by 40% in 2050 [1,2]. Ammonia based fertilizers aid in increasing the food supply for the growing global population (~10 billion by 2050) [3]. Ammonia can also play a major role in the development of a clean transportation sector and can be utilized directly in ammonia fuel cells or indirectly in hydrogen fuel cells. Using state of the art carbon fiber storage tanks, it takes 700 bar pressure to achieve a volumetric energy density of 5.3 GJ m^{-3} for hydrogen. With ammonia, liquefaction is achieved under 10 bar pressure and yields 13.6 GJ m^{-3} energy density. Ammonia can be a superior energy carrier of hydrogen compared to other conventional fuels (e.g., the hydrogen content in liquid ammonia is 17.6 wt% compared with 12.5 wt% for methanol) [4,5]. Thus, sustainable ammonia production lies at the nexus of food-energy chemistry.

The fixation of nitrogen to ammonia is a complex multi-step reaction, due to the high bonding energy of diatomic nitrogen (N≡N bond energy of 940.95 kJ mol^{-1}) [6]. Currently, ammonia synthesis is heavily dependent upon the Haber-Bosch process, which converts nitrogen and hydrogen to ammonia ($N_2 + 3H_2 \rightarrow 2NH_3$). This process is energy-intensive (> 600 kJ mol^{-1} ammonia), requiring high operating temperatures and pressures (150–350 atm, 350–550 °C). In the Haber-Bosch process, all of the hydrogen gas is produced by the steam reformation of natural gas ($CH_4 + 2H_2O \rightarrow 4H_2 + CO_2$). This consumes 3–5% of the global natural gas supply and is responsible for 450 million metric tons of CO_2 emission annually [7,8]. This mandates an alternative approach for sustainable and scalable ammonia synthesis under ambient conditions that can alleviate extreme condition requirements. Electrocatalytic fixation of nitrogen is a form of artificial synthesis that mimics the natural nitrogen enzymatic process [9]. The electrochemical nitrogen reduction reaction (NRR) enables the decentralized production of ammonia at ambient conditions from N_2, H_2O, and electricity, which

* Corresponding author.
E-mail address: melsayed@gatech.edu (M.A. El-Sayed).

https://doi.org/10.1016/j.nanoen.2018.04.039
Received 24 March 2018; Received in revised form 14 April 2018; Accepted 14 April 2018
Available online 22 April 2018

can be provided through renewable energy sources (e.g., solar) that are readily available from the environment [10,11]. To date, few studies have been carried out to explore the fixation of nitrogen to ammonia using various electrocatalytic approaches [12–16]. Unfortunately, in most of these studies, the ammonia yield and faradaic efficiency were too low to be practical for fertilizer production, mainly due to the stability of the N_2 triple bond and to intrinsic competition with the hydrogen evolution reaction (HER). Furthermore, using molten salt systems and electrochemical lithium cycling strategy results in higher ammonia yield and faradaic efficiency; however, they are not energetically efficient and require high temperatures [17,18]. Developing an efficient heterogeneous electrocatalyst to remarkably increase the rate of ammonia production and faradaic efficiency through an energy efficient and environmentally friendly technique is vital in energy and agriculture-based industries.

Previous theoretical and experimental studies have shown the greater performance for electrochemical NRR using Au as an electrocatalyst [19–21]. It was proved that NRR on Au surfaces follows an associative mechanism in which the breaking of the triple bond of N_2 and the hydrogenation of the N atoms occur simultaneously [19]. Furthermore, the greater rate of NRR on gold surfaces than on the surfaces of other electrocatalysts is due to its multifaceted Au surfaces, composed of various active sites for N_2 adsorption and reduction [20,21]. The selectivity of N_2 molecules on the surface of nanocatalysts has been demonstrated to be one of the major challenges in electrochemical NRR [22,23]. Here, we aim to enhance the rate of electrochemical NRR under ambient conditions, notably using hollow Au nanocages (AuHNCs) as an effective electrocatalyst. Using AuHNCs, the highest ammonia yield and faradaic efficiency are achieved which are greater than the highest reported values in the literature in aqueous solution under room temperature (20 °C) and atmospheric pressure (Table S2). The catalytic efficiency of AuHNCs are compared with similar concentrations of solid Au nanocubes (AuNCs), nanospheres (AuNSs), and nanorods (AuNRs) to prove that the enhanced rate of NRR using hollow nanocages is due to the increased surface area and the confinement of reactants in the cavity (cage effect).

In nanocatalysis by solid nanoparticles, the catalytic reaction occurs by involving the atoms from the outer surface of the nanocatalyst, while for hollow nanocatalysts the reaction occurs at both the outer and inner surfaces [24–31]. Therefore, the reaction is accelerated in the hollow nanocatalyst because it has a larger active surface area. Reactions in the cavity of the hollow nanocatalyst are facilitated by the confinement of the reactants in the cage (cage effect), which could increase the steady-state concentration of the species in the rate-determining step of the reaction. Additionally, in some cases, the inner surface might not be as well capped with the capping agent as the outer surface and may thus be more catalytically active. In this case, the rate of the reaction increases due to the confinement of the reactants inside the cage [32–34].

2. Results and discussion

Here, AuHNCs are prepared from a silver solid nanocube (AgNC) template by the galvanic replacement technique [30,35,36]. In this method the sacrificial metal template (i.e., Ag) is replaced with the nanocage metal (i.e., Au) if the oxidation potential of the metal template is higher than that of the nanocage metal. The replacement of three Ag atoms of the template with one Au atom ($3Ag_{(s)} + AuCl_4^-{}_{(aq.)} \rightarrow Au_{(s)} + 3Ag^+_{(aq.)} + 4Cl^-_{(aq.)}$) creates a hollow structure with holes at the wall and corners of the nanocage. The size of the AuHNCs is tuned by varying the size of the AgNCs. AgNCs with localized surface plasmon resonance (LSPR) at 429 nm are prepared by a modified polyol reduction method (Fig. 1**A**). The AgNCs are then washed with acetone, centrifuged (10,000 rpm, 10 min) and dispersed in DI water. Hydrogen tetrachloroaurate (0.5 mM) in DI water is injected into the AgNC solution under vigorous stirring (600 rpm) until the peak LSPR spectrum of the solution shifts to 660 nm (Fig. 1**A**). The X-ray diffraction (XRD) pattern of AuHNCs deposited on the Si substrate is composed of various surface index facets that provide active sites for electrochemical NRR (Fig. 1**B**). The average edge length of AuHNCs is 35 nm, obtained from transmission electron microscopy (TEM) analysis (Fig. 1**C, D**).

Electrochemical NRR experiments are conducted in H-type cells where anodic and cathodic compartments are separated by a proton conductive cation exchange membrane (Fig. 2**A**). The electrolyte is 0.5 M $LiClO_4$ aqueous solution (Detailed information about the electrochemical measurement is provided in the Supporting information). Perchlorate anion (ClO_4^-) is selected for NRR due to the minimal and unselective adsorption of the ClO_4^- on the low index facets of Au nanoparticles surface [37]. Li^+ is selected for its superior ability to activate N_2 at ambient conditions [16,18]. The primary reaction at the anodic compartment is:

$$3H_2O \rightarrow \frac{3}{2}O_2 + 6H^+ + 6e^- \quad (1)$$

where water is oxidized to produce oxygen gas and protons (H^+). The protons produced at the anode are transported through the proton conductive membrane to the cathode part where supplied N_2 gas and protons will produce NH_3:

$$N_2 + 6H^+ + 6e^- \rightarrow 2NH_3 \quad (2)$$

The overall reaction is:

$$N_2 + 3H_2O \rightarrow 2NH_3 + \frac{3}{2}O_2 \quad (3)$$

Linear sweep voltammetry (LSV) tests are performed in an Ar and N_2 saturated environment to qualitatively distinguish between HER and NRR (Fig. 2**B**). As the potential moves below − 0.4 V vs. RHE, a notable enhancement in current density is observed under the N_2 saturated environment. This is attributed to the reaction between AuHNCs as a cathodic electrocatalyst and N_2 to produce NH_3. The greatest difference in the LSV curves of N_2 and Ar saturated environments is found at the potential between − 0.4 V to − 0.8 V vs. RHE, at which it is expected that the highest NRR activity in this potential range will be achieved. Moving toward potentials more negative than − 0.8 V vs. RHE yields no further difference in current density between Ar and N_2 (Fig. 2**B**). This indicates that HER is the only reaction at the cathode. Chronoamperometry (CA) tests at a series of potentials are conducted to determine the ammonia yield rate and Faradaic efficiency (Fig. 2**C,** Fig. S1). The calibration curve for the ammonia assay using the Nessler reagent is shown in Fig. S2. The electrochemical NRR obtains higher selectivity within the potential range of − 0.4 V to − 0.6 V vs. RHE, with the highest ammonia yield rate (3.98 μg cm^{-2} h^{-1}) at − 0.5 V and Faradaic efficiency (30.2%) at − 0.4 V. Although in this potential range (− 0.4 V to − 0.6 V), the ammonia yield rate increases as the negative applied potential increases, Faradaic efficiency decreases, which is attributed to the compromise between increasing current density and competitive selectivity toward HER rather than NRR. It is known that H atoms occupy the active sites on Au that prevents N_2 adsorption and reduction on the catalytic surface [21,38]. At negative applied potential below − 0.6 V, both ammonia yield rate and Faradaic efficiency decrease considerably (ammonia yield rate: 1.54 μg cm^{-2} h^{-1}, Faradaic efficiency: 1.1% at − 0.8 V vs. RHE), which suggests that HER is the dominant reaction at the cathode (Fig. 2**C**). To evaluate the durability of AuHNCs, CA tests are performed at − 0.4 V vs. RHE for 5 consecutive cycles, each for 12 h. (Fig. S3). The electrocatalyst shows an excellent stability with a minor decrease in ammonia yield rate and Faradaic efficiency (93.8% performance retention) after the 5th recycling tests (Fig. 2**D**).

To further verify the electrochemical NRR activity using AuHNCs, extensive control experiments are carried out with Ar gas and with no potential applied to the electrodes under N_2 gas (open circuit voltage). Under conditions similar to those in Fig. 2C, except using Ar gas instead of N_2 and with N_2 but no potential applied, significantly smaller

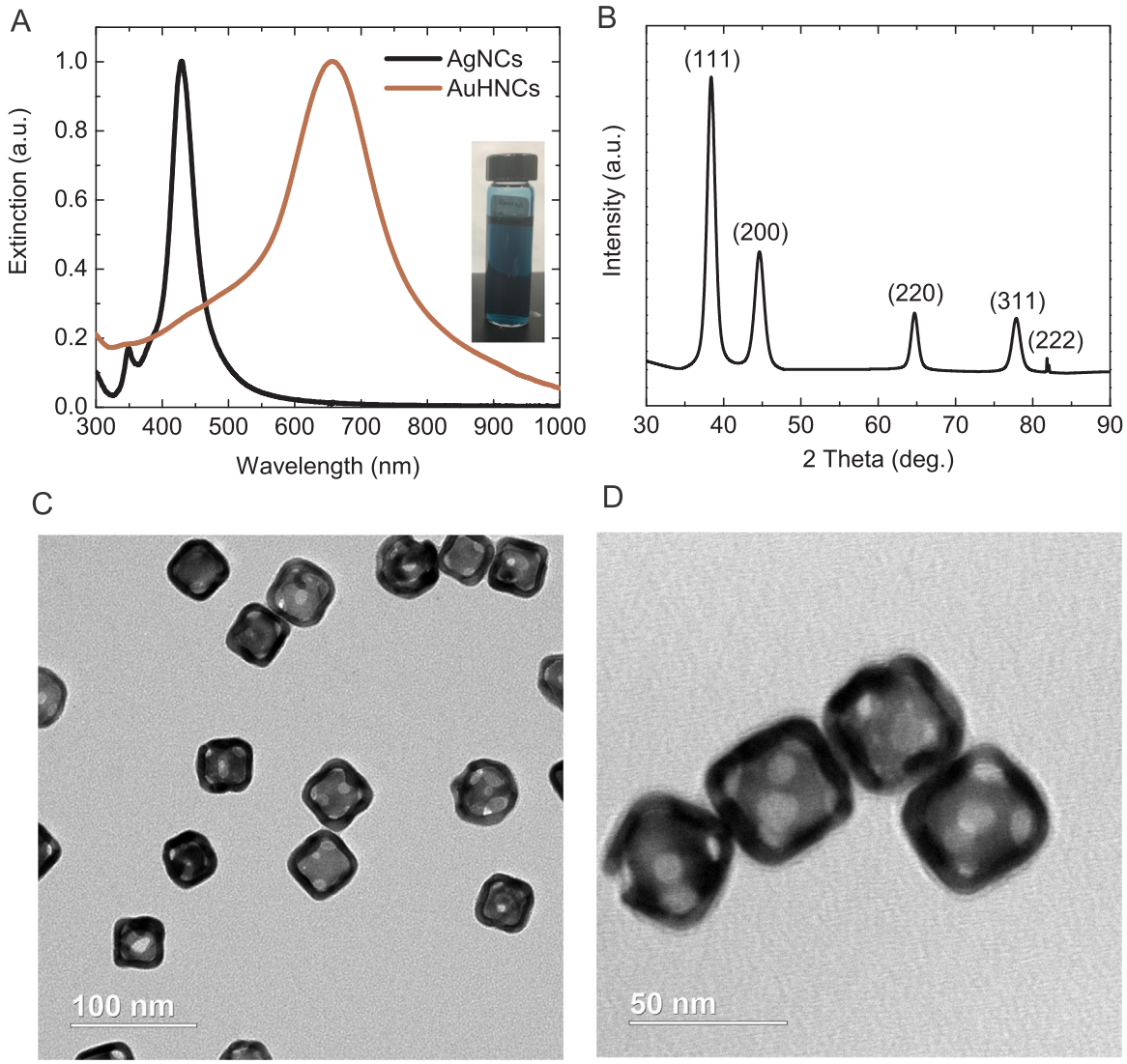

Fig. 1. A) UV–vis extinction spectra of the AgNCs and AuHNCs, the photograph shown in the inset is AuHNCs dispersed in DI water. **B**) XRD pattern of AuHNCs deposited on Si substrate. **C**) and **D)** are the TEM images of AuHNCs with different magnifications. The average edge length of the AuHNCs is 35 nm.

amounts of NH_3 yield are achieved (Fig. S4). This confirms that the results with the N_2 gas under applied potential are not due to the sources of contamination (e.g., laboratory, equipment, membrane). The formation of ammonia during the electrochemical NRR experiments is further validated by surface-enhanced Raman spectroscopy (SERS) [39,40]. Here, the solution collected from the electrochemical experiment, which showed the highest ammonia Faradaic efficiency (− 0.4 V vs. RHE at 20 °C), was mixed with AuNCs, and the SERS spectrum was collected under 785 nm laser excitation (Fig. S5). We also conducted a control experiment, where we collected the SERS spectrum for 0.5 M $LiClO_4$ under the same operating condition, as the SERS band corresponds to the ligand molecules on the AuNCs surface; as well, $LiClO_4$ could possibly interfere with the Raman features of ammonia. In comparison to the SERS spectra collected from the control experiment, a new Raman band at 3062 cm^{-1} appeared for the sample analyzed after the electrochemical experiment, which is attributed to the NH_4^+ moiety present in the electrolyte [41,42]. This was further validated by collecting the Raman spectrum from crystalline NH_4F, which showed a corresponding mode of vibration for NH_4^+ at around 3075 cm^{-1}. The observed shift in the Raman band corresponds to NH_4^+ in SERS spectrum in comparison to the normal Raman spectrum could be attributed to the plasmon-enhanced electromagnetic field effect as well as the modifications in the adsorption (physisorption and chemisorption) orientation of these molecules at the nanoparticle surface. This result points towards the fact that ammonia formed during the electrochemical experiment largely exists as ammonium ions (NH_4^+) in the electrolyte. Furthermore, ^1H NMR spectra obtained from the sample in the NRR experiment lie at a chemical shift of triplet coupling of $^{14}N_2$ similar to that of standard $^{14}NH_4^+$ samples (J-coupling : 52 Hz), which further confirms that the ammonia formation is solely originated from N_2 (Fig. S6). The ammonia production at − 0.4 V vs. RHE at 20 °C quantified from the ^1H NMR analysis is 38.6 μM (see calibration curve in the SI, Fig. S6). This is compared with 41.5 μM of ammonia, measured by UV–Vis spectra using Nessler's test.

By increasing the concentration of AuHNCs from 0.9 μg mL^{-1} to 1.8 μg mL^{-1} (Fig. S7) on the ITO substrate (1 cm^2) at − 0.5 V vs. RHE, both the ammonia yield rate and the Faradaic efficiency increase from 1.88 μg cm^{-2} h^{-1} and 3.12% to 3.98 μg cm^{-2} h^{-1} and 14.8% (Fig. 3**A,** Fig. S8). This is due to the increase in the number of nanoparticles participating in the NRR, which results in an increase in the total active surface area on the substrate. By increasing the electrochemical NRR temperature from 20 °C to° 50 °C at − 0.4 V vs. RHE, the ammonia yield rate and Faradaic efficiency increase from 2.35 μg cm^{-2} h^{-1} and 30.22% to 2.82 μg cm^{-2} h^{-1} and 40.55% (Fig. 3**B,** Fig. S9). Based on the Arrhenius equation, the reaction rate increases exponentially with the temperature (See the Supporting information for the rate constant and

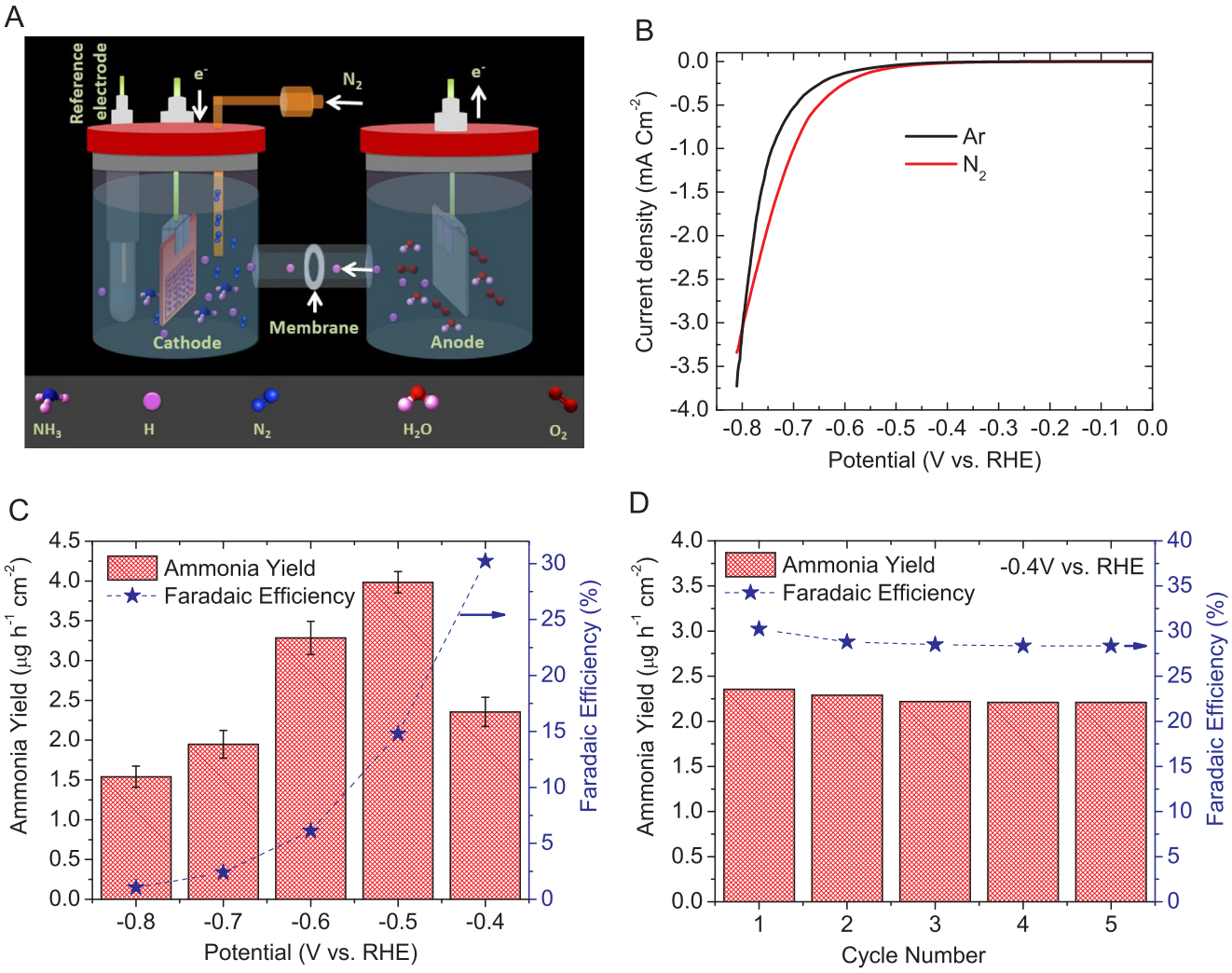

Fig. 2. A) Schematic of electrochemical cell for NRR. The anode and cathode compartments are separated by a cation exchange membrane (CEM). **B)** Linear sweep voltammetry tests in an Ar and N_2 saturated environment in 0.5 M $LiClO_4$ aqueous solution under ambient conditions. **C)** Ammonia yield rate and faradaic efficiency at various potentials in 0.5 M $LiClO_4$ at 20 °C, **D)** Cycling stability results of ammonia yield rate on AuHNCs. For each cycle CA test was carried out at − 0.4 V vs. RHE in 0.5 M $LiClO_4$ at 20 °C.

activation energy calculation). The mass transport rate is faster at higher temperatures, while the N_2 solubility decreases at higher temperatures. For these experiments, faster kinetics plays a major role in enhancing the NRR rate at higher temperatures. The ammonia yield rate and Faradaic efficiency can be further enhanced by using ionic liquids (e.g., [C4mpyr][eFAP]) that offer significantly higher N_2 solubility compared to the aqueous solution [43].

To further investigate the cage effect using AuHNCs, the NRR rate is

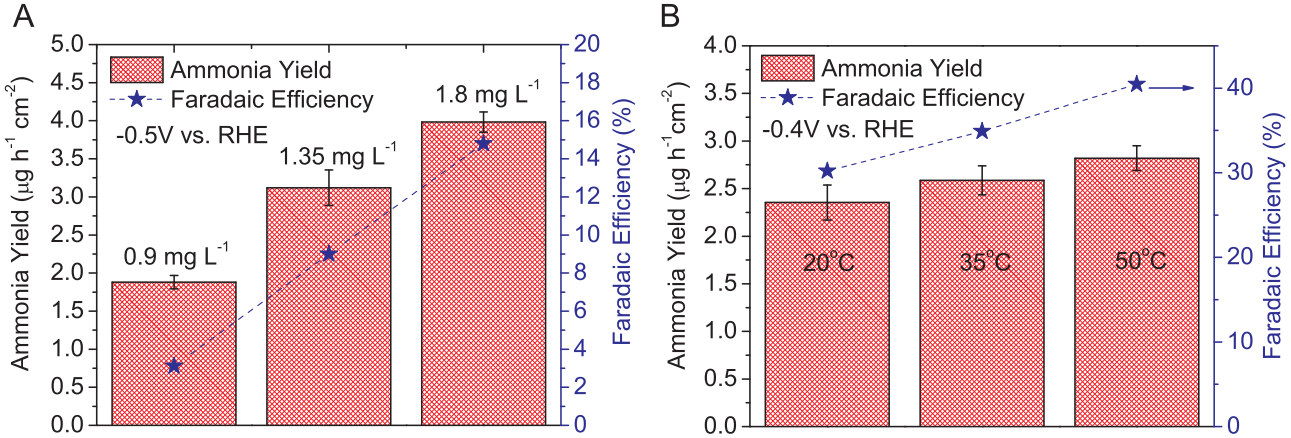

Fig. 3. A) Ammonia yield rate and faradaic efficiency of AuHNCs at various concentrations at − 0.5 V vs. RHE in 0.5 M $LiClO_4$ aqueous solution under ambient conditions. **B)** Ammonia yield rate and faradaic efficiency of AuHNCs at various temperatures at − 0.4 V vs. RHE in 0.5 M $LiClO_4$ aqueous solution.

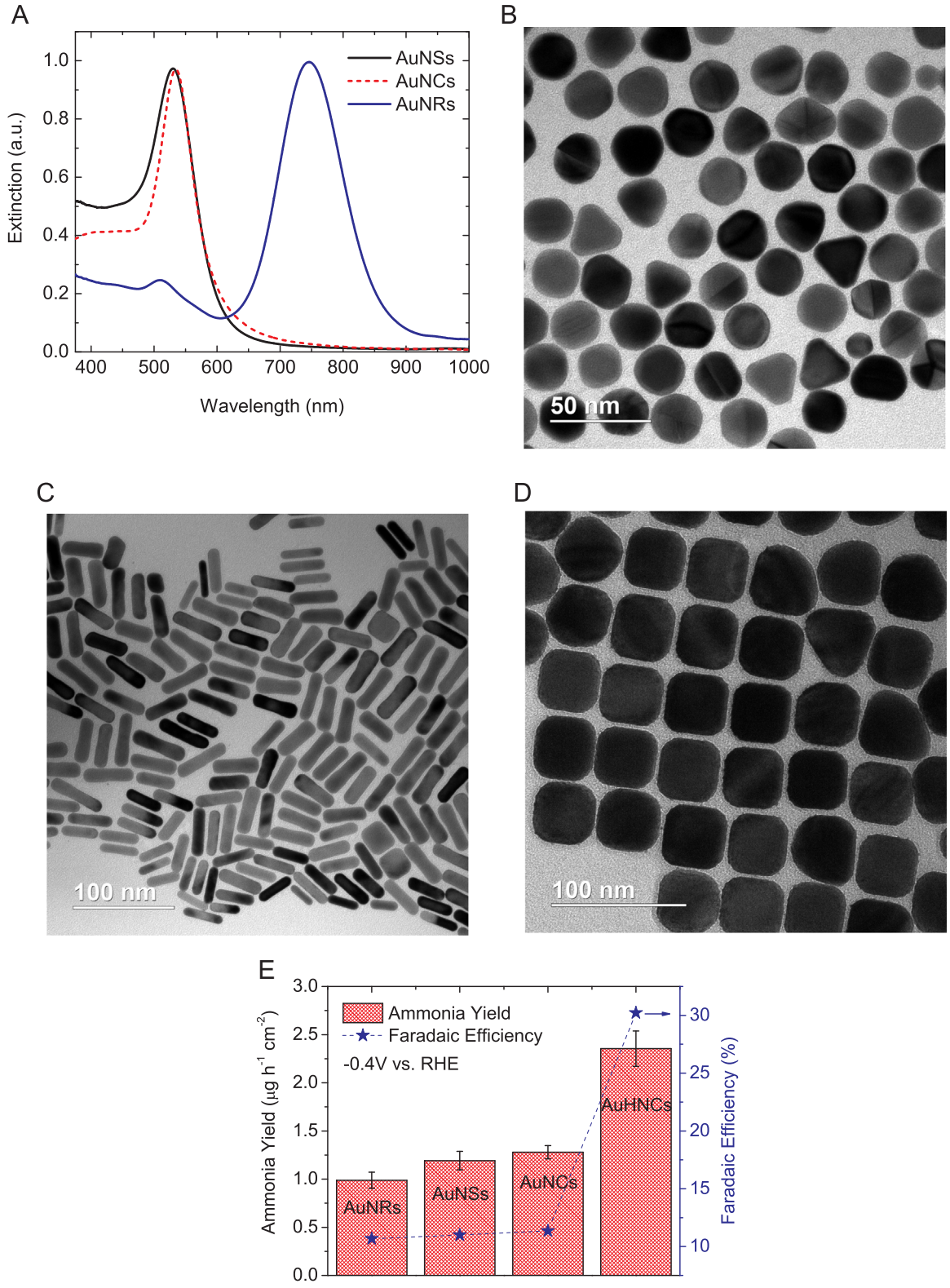

Fig. 4. A) UV–vis extinction spectra of AuNSs, AuNCs, and AuNRs, **B**), **C**), and **D**) are the TEM images of AuNSs, AuNRs, and AuNCs, respectively. **E**) Ammonia yield rate and Faradaic efficiency for nanoparticles of various types and shapes at the potential of − 0.4 V vs. RHE in 0.5 M $LiClO_4$ aqueous solution.

evaluated using solid Au nanoparticles of various shapes (i.e., rods, spheres, cubes) with similar nanoparticle concentrations (see Supporting information for the detailed calculation of nanoparticle concentration). The LSPR of AuNSs and AuNCs lies at 535 nm and two plasmon peaks for AuNRs are observed which are attributed to the transverse (512 nm) and longitudinal (746 nm) modes (Fig. 4**A**). The average diameter and edge length of AuNSs and AuNCs, respectively are 35 nm while AuNRs have an average length and width of 42 nm and 12 nm as obtained from TEM images (Fig. 4**B–D**). The ammonia yield rate and Faradaic efficiency are significantly lower using solid Au nanoparticles compared to the AuHNCs (Fig. 4**E**, Fig. S10). The lowest ammonia yield rate and Faradaic efficiency are obtained for AuNRs

(0.99 μg cm^{-2} h^{-1}, 10.69%). A minor increase in the NRR rate is observed using AuNSs (ammonia yield rate: 1.19 μg cm^{-2} h^{-1}, Faradaic efficiency: 11%) and AuNCs (ammonia yield rate: 1.27 μg cm^{-2} h^{-1}, Faradaic efficiency: 11.35% for AuNCs). This is in accordance with our previous findings, which suggest that nanoparticles with sharper edges and corners yield higher catalytic activity [32]. This is due to the increased number of valency-unsatisfied surface atoms (atoms that do not have the full number of bonds that they can chemically accommodate) in nanoparticles with sharper edges, providing more active sites for catalytic reaction than smoother nanoparticles [32]. The significant enhancement in the NRR rate using AuHNCs is attributed to the entrapment of N_2 molecules within the cavity, as these likely experience high frequency collisions with the hollow Au interior surface of the cages. This increases the residence time of N_2 molecules on the nanoparticle inner surface, which facilitates the conversion of N_2 to NH_3. In addition, the presence of less capping material (i.e., polyvinylpyrrolidone (PVP)) on the inner surface than the outer surface of the AuHNCs can enhance the NRR catalytic activity.

3. Conclusion

Electrocatalytic activity of NRR under ambient conditions was studied using AuHNCs as an effective electrocatalyst in 0.5 M $LiClO_4$ aqueous solution. The highest ammonia yield rate (3.9 μg cm^{-2} h^{-1}) is achieved at − 0.5 V vs. RHE, while the highest ammonia Faradaic efficiency (30.2%) is obtained at − 0.4 V vs. RHE using AuHNCs. At higher applied potentials, both ammonia yield rate and Faradaic efficiency decrease due to the intrinsic competition between NRR and HER. By increasing the electrochemical operating temperature from 20 °C to 50 °C at − 0.4 V vs. RHE, the ammonia yield rate and Faradaic efficiency were improved to 2.82 μg cm^{-2} h^{-1} and 40.55% from 2.35 μg cm^{-2} h^{-1} and 30.2%, which is attributed to the faster mass transport rate. By increasing the concentration of AuHNCs from 0.9 μg mL^{-1} to 1.8 μg mL^{-1} on the ITO substrate, the ammonia yield rate and Faradaic efficiency increased from 1.88 μg cm^{-2} h^{-1} and 3.12% to 3.98 μg cm^{-2} h^{-1} and 14.8% at − 0.5 V vs RHE. It was demonstrated that due to the increase in the surface area, the higher number of successful collisions of reactants with the interior Au surface in the cavity (cage effect), and presence of less capping materials inside the cavity, AuHNCs offer superior electrocatalytic activity (three-fold enhancement) compared to the solid nanoparticles with the same concentration.

The unique electrocatalytic activity of AuHNCs in NRR can open a new avenue for clean and sustainable ammonia electrosynthesis from N_2 and water under ambient conditions with high ammonia yield rate and Faradaic efficiency.

4. Experimental section

4.1. Nanoparticle Synthesis

4.1.1. Preparation of AgNCs and AuHNCs

Hollow gold nanoparticles with cubic shape are prepared by the galvanic replacement method using cubic silver nanoparticles as a template. Silver nanocubes (AgNCs) are prepared by a modified polyol reduction of $AgNO_3$. In a 100 mL round-bottomed flask, 35 mL of anhydrous ethylene glycol (EG) is stirred at 400 rpm and heated at 150 °C for 1 h in an oil bath. After 1 h heating of the EG, 0.35 gr of polyvinylpyrrolidone (PVP, MW ~ 55000) dissolved in 5 mL EG is added at once to the reaction mixture. The temperature of the reaction mixture is then increased gradually until it reaches 155 °C. At this temperature, 0.4 mL of 3 mM solution of sodium sulfide ($Na_2S{\cdot}9H_2O$) in EG is added 5 min after the addition of PVP. The solution of sodium sulfide must be prepared an hour before injection into the reaction mixture. Finally, 0.25 g of $AgNO_3$ dissolved in 5 mL of EG is added at once with stirring set to 200 rpm until the color changes from brownish yellow to pale yellow. Then the stirring and heating are stopped and the solution temperature is allowed to decrease to room temperature. To clean the AgNCs solution from the byproducts, extra PVP, and organic solvents, 20 mL of the AgNCs solution is diluted with 20 mL of acetone and centrifuged for 10 min at 10,000 rpm. The precipitated AgNCs are dispersed in the solution of 0.01 g PVP dissolved in 100 mL of DI water. To prepare AuHNCs, the cleaned AgNCs solution in DI water is heated and brought to boiling. Then, $HAuCl_4$ (0.2 g L^{-1}) in DI water is injected to the AgNC solution under vigorous stirring (600 rpm) until the peak LSPR spectrum of the solution shifts to 660 nm. The solution is refluxed for 2 min with stirring until the LSPR remains fixed. The solution is cooled down and centrifuged at 10,000 rpm for 10 min. The precipitated nanoparticles are dispersed in DI water for future use.

4.1.2. Preparation of AuNSs

AuNSs are prepared by the reduction of $HAuCl_4{\cdot}3H_2O$ using PVP (MW ~ 10,000) that acts as both a capping and a reducing agent. In a 150 mL flask, 100 mL of 0.085 mM $HAuCl_4$ in DI water is heated and brought to boiling. Under 500 rpm stirring, 0.65 g PVP is added. The reaction is allowed to proceed until the solution turns to red color and the LSPR peak becomes narrow. The solution is cooled down and centrifuged at 10,000 rpm for 10 min. The precipitated nanoparticles are dispersed in DI water for future use.

4.1.3. Preparation of AuNCs

AuNCs are prepared using a modified surfactant-directed seed-mediated approach [44]. The seed particles are prepared using 7.75 mL of solution containing 7.50 mL of 0.1 M cetyltrimethylammonium bromide (CTAB) and 0.25 mL of 0.01 M $HAuCl_4$ in DI water. Next, 0.6 mL of an ice cold 0.01 M $NaBH_4$ solution is added to the initial solution for the subsequent reduction of gold ions. The resulting solution is stirred for 2 min and remains undisturbed for an hour before use. The seed solution is then diluted 10 times with DI water. To prepare the growth solution, 4 mL of DI water, 0.8 mL of 0.1 M CTAB, and 0.1 mL of 0.01 M $HAuCl_4$ are mixed thoroughly. A 0.6 mL of 0.1 M ascorbic acid is added to the growth solution and mixed thoroughly until the solution turns colorless. Finally, 2.5 μL of the diluted seed solution is added to the growth solution and the reaction vessel is allowed to sit overnight. The AuNCs are centrifuged two times at 10,000 rpm for 10 min. The precipitated AuNCs are dispersed in DI water for future use.

4.1.4. Preparation of AuNRs

AuNRs are synthesized by the modified seed-mediated protocol [45]. Briefly, the seed nanoparticles are prepared by adding 0.25 mL of $HAuCl_4$ (0.01 M) to 7 mL of CTAB (0.1 M) followed by the addition of 0.01 M of ice-cold $NaBH_4$ (0.6 mL) solution in DI water. This solution is stirred for 2 min and left undisturbed for 1 h. In the subsequent step, 1 mL of seed solution is added to the growth solution, which is prepared by mixing 100 mL of CTAB (0.1 M) with 4.25 mL of $HAuCl_4$ (0.01 M), 0.625 mL of $AgNO_3$ (0.01 M), and 0.675 mL of ascorbic acid (0.1 M). After the addition of the seed solution, the entire solution is kept undisturbed for 12 h. The resultant AuNRs are purified by centrifugation (10,000 rpm for 10 min) and redispersed in DI water.

4.2. Electrochemical measurement

In order to prepare a working electrode (cathode), 300 μL of nanoparticles of known concentration and 1.5 μL of nafion solution (5% wt.) were sonicated and dropped onto a indium tin oxide (ITO) (1 cm × 1 cm) and then dried under N_2 atmosphere at 75 °C for 45 min. Electrochemical measurements were carried out at 20 °C, 35 °C, and 50 °C in the water bath in 0.5 M $LiClO_4$ electrolyte (40 mL, each side) using a CHI instrument potentiostat (CHI, 700D) in the three-electrode setup. Pt mesh (1 cm × 1 cm) and Ag/AgCl reference electrode (3 M, BASi, USA) were used as counter and reference electrodes. CEM was used to separate the anodic and cathodic compartments while protons produced at the anode can transport across the membrane to the

cathode side where NRR occurs.

The measured potentials vs. Ag/AgCl are iR-compensated and converted to the reversible hydrogen electrode (RHE) scale based on the following equation:

$$E_{RHE} = E_{Ag/AgCl} + \frac{2.3RT}{F}PH + E^{o}_{Ag/AgCl} \quad (4)$$

where E_{RHE} is the converted potential vs. RHE, $E^{o}_{Ag/AgCl} = 0.2027$ at 20 °C with the slope of $-1.01\,mV/^{o}C$, $E_{Ag/AgCl}$ is the experimentally measured potential against Ag/AgCl reference electrode, R is the gas constant ($8.314\,J\,mol^{-1}\,K^{-1}$), and T is the operating temperature (K). The electrolyte is fed with N_2 or Ar gas for 2 h before starting the measurement at the flow rate of $20\,mL\,min^{-1}$.

Acknowledgements

This work is supported by National Science Foundation, Division of Chemistry, CHE-1608801 (electrochemical and spectroscopy phenomena) and US Department of Energy, Office of Basic Energy Sciences, Division of Materials Sciences and Engineering under Award no. DE-FG02-09ER46604 (plasmonic nanostructures). Materials characterization was performed at the Georgia Tech Institute for Electronics and Nanotechnology (IEN), a member of the National Nanotechnology Coordinated Infrastructure, which is supported by the National Science Foundation (Grant ECCS-1542174).

Supporting information

More detailed information regarding the ammonia quantification, calculation of ammonia Faradaic efficiency, determination of nanoparticle concentration, activation energy calculations, and instrumentation are provided in the supporting information.

Appendix A. Supporting information

Supplementary data associated with this article can be found in the online version at http://dx.doi.org/10.1016/j.nanoen.2018.04.039.

References

[1] U. G. Survey, O. S, and U. G. Survey, Mineral Commodity Summaries, 2009: Government Printing Office, 2009.
[2] H.J. van Grinsven, L. Bouwman, K.G. Cassman, H.M. van Es, M.L. McCrackin, A.H. Beusen, Losses of ammonia and nitrate from agriculture and their effect on nitrogen recovery in the European Union and the United States between 1900 and 2050, J. Environ. Qual. 44 (2015) 356–367.
[3] U.N.D.o. Economic, World population prospects: The 2006 revisionvol. 261: United Nations Publications, 2007.
[4] T. Hua, R. Ahluwalia, J.-K. Peng, M. Kromer, S. Lasher, K. McKenney, K. Law, J. Sinha, Technical assessment of compressed hydrogen storage tank systems for automotive applications, Int. J. Hydrog. Energy 36 (2011) 3037–3049.
[5] D.J. Little, M.R. Smith III, T.W. Hamann, Electrolysis of liquid ammonia for hydrogen generation, Energy Environ. Sci. 8 (2015) 2775–2781.
[6] K. Honkala, A. Hellman, I. Remediakis, A. Logadottir, A. Carlsson, S. Dahl, C.H. Christensen, J.K. Nørskov, Ammonia synthesis from first-principles calculations, Science 307 (2005) 555–558.
[7] V. Smil, Enriching the Earth: Fritz Haber, Carl Bosch, and the Transformation of World Food Production, MIT Press, 2004.
[8] R. Strait, M. Nagvekar, Carbon dioxide capture and storage in the nitrogen and syngas industries, Nitrogen+ Syngas 303 (2010) 1–3.
[9] T. Spatzal, M. Aksoyoglu, L. Zhang, S.L. Andrade, E. Schleicher, S. Weber, D.C. Rees, O. Einsle, Evidence for interstitial carbon in nitrogenase FeMo cofactor, Science 334 (2011) (pp. 940-940).
[10] X. Chen, N. Li, Z. Kong, W.-J. Ong, X. Zhao, Photocatalytic fixation of nitrogen to ammonia: state-of-the-art advancements and future prospects, Mater. Horiz. 5 (2018) 9–27.
[11] A.J. Medford, M.C. Hatzell, Photon-driven nitrogen fixation: current progress, thermodynamic considerations, and future outlook, ACS Catalysis 7 (2017), pp. 2624–2643.
[12] S. Mukherjee, D.A. Cullen, S. Karakalos, K. Liu, H. Zhang, S. Zhao, H. Xu, K.L. More, G. Wang, G. Wu, Metal-organic framework-derived nitrogen-doped highly disordered carbon for electrochemical ammonia synthesis using N_2 and H_2O in alkaline electrolytes, Nano Energy (2018).
[13] R. Lan, J.T. Irvine, S. Tao, Synthesis of ammonia directly from air and water at ambient temperature and pressure, Sci. Rep. 3 (2013) 1145.
[14] Y. Liu, Y. Su, X. Quan, X. Fan, S. Chen, H. Yu, H. Zhao, Y. Zhang, J. Zhao, Facile ammonia synthesis from electrocatalytic N2 reduction under ambient conditions on N-doped porous carbon, ACS Catal. (2018).
[15] S. Chen, S. Perathoner, C. Ampelli, C. Mebrahtu, D. Su, G. Centi, Electrocatalytic synthesis of ammonia at room temperature and atmospheric pressure from water and nitrogen on a carbon-nanotube-based electrocatalyst, Angew. Chem. 129 (2017) 2743–2747.
[16] G.-F. Chen, X. Cao, S. Wu, X. Zeng, L.-X. Ding, M. Zhu, H. Wang, Ammonia electrosynthesis with high selectivity under ambient conditions via a Li+ incorporation strategy, J. Am. Chem. Soc. 139 (2017) 9771–9774.
[17] S. Licht, B. Cui, B. Wang, F.-F. Li, J. Lau, S. Liu, Ammonia synthesis by N2 and steam electrolysis in molten hydroxide suspensions of nanoscale Fe2O3, Science 345 (2014) 637–640.
[18] J.M. McEnaney, A.R. Singh, J.A. Schwalbe, J. Kibsgaard, J.C. Lin, M. Cargnello, T.F. Jaramillo, J.K. Nørskov, Ammonia synthesis from N2 and H2O using a lithium cycling electrification strategy at atmospheric pressure, Energy Environ. Sci. 10 (2017) 1621–1630.
[19] Y. Yao, S. Zhu, H. Wang, H. Li, M. Shao, A spectroscopic study on the nitrogen electrochemical reduction reaction on gold and platinum surfaces, J. Am. Chem. Soc. (2018).
[20] M.M. Shi, D. Bao, B.R. Wulan, Y.H. Li, Y.F. Zhang, J.M. Yan, Q. Jaing, Au sub--nanoclusters on TiO2 toward highly efficient and selective electrocatalyst for N2 conversion to NH3 at ambient conditions, Adv. Mater. 29 (2017).
[21] D. Bao, Q. Zhang, F.L. Meng, H.X. Zhong, M.M. Shi, Y. Zhang, J. Yan, Q. Jiang, X. Zhang, Electrochemical reduction of N2 under ambient conditions for artificial N2 fixation and renewable energy storage using N2/NH3 cycle, Adv. Mater. 29 (2017).
[22] J.H. Montoya, C. Tsai, A. Vojvodic, J.K. Nørskov, The challenge of electrochemical ammonia synthesis: a new perspective on the role of nitrogen scaling relations, ChemSusChem 8 (2015) 2180–2186.
[23] A.R. Singh, B.A. Rohr, J.A. Schwalbe, M. Cargnello, K. Chan, T.F. Jaramillo, I. Chorkendorff, J.K. Nørskov, Electrochemical Ammonia Synthesis· The Selectivity Challenge, ACS Publications, 2016.
[24] T.S. Ahmadi, Z.L. Wang, T.C. Green, A. Henglein, M.A. El-Sayed, Shape-controlled synthesis of colloidal platinum nanoparticles, Science (1996) 1924–1925.
[25] R. Narayanan, M.A. El-Sayed, Shape-dependent catalytic activity of platinum nanoparticles in colloidal solution, Nano Lett. 4 (2004) 1343–1348.
[26] R. Narayanan, M.A. El-Sayed, Effect of colloidal nanocatalysis on the metallic nanoparticle shape: the Suzuki reaction, Langmuir 21 (2005) 2027–2033.
[27] M. Mahmoud, F. Saira, M. El-Sayed, Experimental evidence for the nanocage effect in catalysis with hollow nanoparticles, Nano Lett. 10 (2010) 3764–3769.
[28] M. Mahmoud, M. El-Sayed, Time dependence and signs of the shift of the surface plasmon resonance frequency in nanocages elucidate the nanocatalysis mechanism in hollow nanoparticles, Nano Lett. 11 (2011) 946–953.
[29] G. Weng, M.A. Mahmoud, M.A. El-Sayed, Nanocatalysts can change the number of electrons involved in oxidation–reduction reaction with the nanocages being the most efficient, J. Phys. Chem. C. 116 (2012) 24171–24176.
[30] Y. Sun, Y. Xia, Shape-controlled synthesis of gold and silver nanoparticles, Science 298 (2002) 2176–2179.
[31] R. Narayanan, M.A. El-Sayed, Changing catalytic activity during colloidal platinum nanocatalysis due to shape changes: electron-transfer reaction, J. Am. Chem. Soc. 126 (2004) 7194–7195.
[32] M.A. Mahmoud, R. Narayanan, M.A. El-Sayed, Enhancing colloidal metallic nanocatalysis: sharp edges and corners for solid nanoparticles and cage effect for hollow ones, Acc. Chem. Res. 46 (2013) 1795–1805.
[33] M.A. Mahmoud, D. O'Neil, M.A. El-Sayed, Hollow and solid metallic nanoparticles in sensing and in nanocatalysis, Chem. Mater. 26 (2013) 44–58.
[34] M.A. Mahmoud, D. O'Neil, M.A. El-Sayed, Shape-and symmetry-dependent mechanical properties of metallic gold and silver on the nanoscale, Nano Lett. 14 (2014) 743–748.
[35] C. Yen, M. Mahmoud, M. El-Sayed, Photocatalysis in gold nanocage nanoreactors, J. Phys. Chem. A 113 (2009) 4340–4345.
[36] J. Chen, B. Wiley, Z.Y. Li, D. Campbell, F. Saeki, H. Cang, et al., Gold nanocages: engineering their structure for biomedical applications, Adv. Mater. 17 (2005) 2255–2261.
[37] J.A. Bordley, M.A. El-Sayed, Enhanced electrocatalytic activity toward the oxygen reduction reaction through alloy formation: platinum–silver alloy nanocages, J. Phys. Chem. C. 120 (2016) 14643–14651.
[38] T. Oshikiri, K. Ueno, H. Misawa, Selective dinitrogen conversion to ammonia using water and visible light through plasmon-induced charge separation, Angew. Chem. 128 (2016) 4010–4014.
[39] P.L. Stiles, J.A. Dieringer, N.C. Shah, R.P. Van Duyne, Surface-enhanced Raman spectroscopy, Annu. Rev. Anal. Chem. 1 (2008) 601–626.
[40] S.R. Panikkanvalappil, M.A. Mackey, M.A. El-Sayed, Probing the unique dehydration-induced structural modifications in cancer cell DNA using surface enhanced Raman spectroscopy, J. Am. Chem. Soc. 135 (2013) 4815–4821.
[41] R.A. Kydd, R.P. Cooney, Raman spectra of adsorbed ammonia on carbon-overlayered silver electrodes, J. Chem. Soc., Faraday Trans. 1: Phys. Chem. Condens. Phases 79 (1983) 2887–2897.
[42] J.-L. Dong, X.-H. Li, L.-J. Zhao, H.-S. Xiao, F. Wang, X. Guo, Y. Zhang, Raman observation of the interactions between NH4+, SO42-, and H2O in supersaturated (NH4) 2SO4 Droplets, J. Phys. Chem. B 111 (2007) 12170–12176.
[43] F. Zhou, L.M. Azofra, M. Ali, M. Kar, A.N. Simonov, C. McDonnell-Worth, C. Sun, X. Zhang, D.R. MacFarlane, Electro-synthesis of ammonia from nitrogen at ambient temperature and pressure in ionic liquids, Energy Environ. Sci. 10 (2017)

2516–2520.
[44] T.K. Sau, C.J. Murphy, Room temperature, high-yield synthesis of multiple shapes of gold nanoparticles in aqueous solution, J. Am. Chem. Soc. 126 (2004) 8648–8649.
[45] B. Nikoobakht, M.A. El-Sayed, Preparation and growth mechanism of gold nanorods (NRs) using seed-mediated growth method, Chem. Mater. 15 (2003) 1957–1962.

Mohammadreza Nazemi is a Ph.D. student at the Laser Dynamics Laboratory under the supervision of Prof. Mostafa A. El-Sayed at Georgia Institute of Technology. He received his BS degree (2013) in Aerospace Engineering from Sharif University of Technology and MS degree (2015) in Mechanical Engineering from Michigan Technological University. His current research focuses on the development and testing of hollow plasmonic nanostructures for photoelectrochemical energy generation. In addition, he is using ultrafast spectroscopy to study the energy transfer in plasmonic nanomaterials and semiconductors.

Sajanlal Panikkanvalappil received his Ph.D. degree in Physical Chemistry from Indian Institute of Technology Madras in 2011. Currently, he is working as a Research Scientist II in the School of Chemistry and Biochemistry at Georgia Institute of Technology. His research focuses on exploring novel routes to synthesize technically relevant nanomaterials, formulating ultrasensitive sensors and developing nanotechnology-based techniques to understand biomolecular events in cancer cells as well as to diagnose and selectively destroy them at its early stages using plasmonic nanoparticles-based techniques. He has authored or co-authored more than 36 well-cited scientific articles including three book chapters, two US patents and ten patent applications, in the most prestigious journals in the fields of material science and nanotechnology.

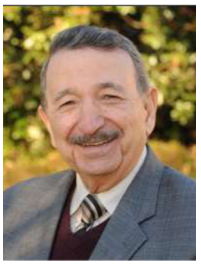

Mostafa A. El-Sayed is the director of the Laser Dynamics Laboratory, Regents' Professor, and Julius Brown Chair in the School of Chemistry and Biochemistry at Georgia Institute of Technology. He obtained his Ph.D. from Florida State University in 1959 with Michael Kasha, and after postdoctoral fellowships at Harvard, Yale, and Caltech, he joined the faculty of School of Chemistry and Biochemistry at UCLA in 1961 and Georgia Tech later in 1994. He is currently an elected member of the U.S. National Academy of Science, an elected fellow of the American Academy of Arts and Sciences, and former editor-in-chief of the Journal of Physical Chemistry. He is the recipient of several prestigious awards including ACS Priestly medal, Ahmed Zewail prize in molecular sciences, the ACS Irving Langmuir Prize in Chemical Physics, the Glenn T. Seaborg Medal, and the U.S. National Medal of Science. He was recently included in the top 1% most cited researchers in 2017 (web of science).